

Determination of Fluid Friction Factor for Nanofluids in Pipes

By:

Mohamad Qayyum bin Mohd Tamam

14596

Dissertation submitted in partial fulfillment of

the requirements for the

Bachelor of Engineering (Hons.)

(Mechanical)

DECEMBER 2014

Universiti Teknologi PETRONAS

Bandar Seri Iskandar

31750 Tronoh

Perak Darul Ridzuan

CERTIFICATION OF APPROVAL

Determination of Fluid Friction Factor for Nanofluids in Pipes

By

Mohamad Qayyum bin Mohd Tamam

14596

A project dissertation submitted to the Petroleum Engineering Programme

Universiti Teknologi PETRONAS

In Partial Fulfilment of the requirement for the

BACHELOR OF ENGINEERING (Hons)

MECHANICAL

Approved by,

.....

(Prof. Dr. Viswanatha Sharma Korada)

Project Supervisor

UNIVERSITI TEKNOLOGI PETRONAS
TRONOH, PERAK
SEPTEMBER 2014

CERTIFICATION OF ORIGINALITY

This is to certify that I am responsible for the work submitted in this project, that the original work is my own except as specified in the references and acknowledgements, and that the original work contained herein have not been undertaken or done by unspecified sources or persons.

MOHAMAD QAYYUM BIN MOHD TAMAM

Mechanical Engineering Department
Universiti Teknologi PETRONAS

ACKNOWLEDGEMENT

First of all, I would like to express my gratefulness and thankfulness to the almighty Allah for his endowment and guidance of which have allowed me to complete my final year project without the presence of unbearable predicaments.

My appreciation extends to my project supervisor, Prof. Dr. Viswanatha Sharma Korada and my co-supervisor, Dr. Subash Kamal whose wisdom and guidance has aided me through difficult problems and ultimately inspired me to brace through towards completion of this project. I would also like to express my gratitude and appreciation for their patience and zealousness to motivate me to never give up.

In addition, I would like to thank Mr. Suleiman Akilu who has sacrificed his time and effort in helping me to conduct the experiments and whose guide and aid has allowed me to run the experiments correctly and smoothly.

I would also like to thank the laboratory staff of Mechanical Engineering Department, specifically Mr. Mohd Kamarul Azlan and Mr. Muhammad Hazri for their relentless efforts of assistance and willingness to aid me in carrying out the experiments. I will always appreciate the opportunity they have provided me in gaining memorable and important experience.

Furthermore, I would also like to express my utmost gratitude towards Mechanical Engineering Department academic and managerial staff specifically Head of Department, Ir. Dr. Masri, Final Year Project course coordinator Dr. Rahmat Iskandar, and not forgetting Ms. Azizah and Mr. Jafni, for their continuous efforts of assistance in terms of project funding. Cooperation on your behalf is very much obliged.

Lastly I would like to thank all those who have supported me during the ups and downs of my research experience, and also the university as a whole to have taught me countless lessons and skills which I recently realised as being crucial for everyday life especially within the industry.

TABLE OF CONTENTS

Chapter	Title	Page
	Table of contents.....	i
	List of figures.....	iii
	List of tables.....	v
	Abstract.....	1
1.0	Introduction.....	2
	1.1 Background of study.....	2
	1.2 Problem statement.....	4
	1.3 Objectives of study.....	4
	1.4 Scope of study.....	4
2.0	Literature review.....	5
	2.1 Introduction to nanofluids.....	5
	2.2 Fabrication of nanoparticles and nanofluids.....	6
	2.3 Applications of nanofluids.....	7
	2.4 Previous related studies on nanoparticle friction factor.....	9
	2.5 Nanoparticles chosen for experiment.....	13
	2.5.1 Silicon Dioxide.....	13
	2.5.2 Titanium Dioxide.....	14
	2.5.3 Zinc Oxide.....	14
3.0	Research methodologies and project activities.....	17
	3.1 Research methodology.....	17
	3.2 Project activities.....	26
	3.3 Gantt chart.....	27
	3.4 Key milestones.....	29
4.0	Theoretical modelling of experiment.....	31
	4.1 Assumptions and Equations used for modelling.....	31
	4.2 Modelling procedures.....	32
	4.3 Results.....	34

5.0	Experimental Results and Discussion.....	36
	5.1 Results for Baseline data (water).....	36
	5.2 Results for nanofluids.....	39
	5.3 Discussion.....	44
6.0	Conclusion and Recommendations.....	46
	References.....	47
	Appendix.....	50

LIST OF FIGURES

1. Figure 1. Moody Chart or Moody Diagram
2. Figure 2. Schematic diagram of experimental apparatus to measure pressure drop as used by Ko et al. (2007)
3. Figure 3. A graph of pressure drop (Pa) against flowrate (m^3/s) for DW, PCNT and TCNT for 1400 ppm CNT loading (Ko et al., 2007)
4. Figure 4. Graphs of friction factor against dimensionless flowrate/Reynolds number for DW as baseline for PCNT and TCNT (Ko et al., 2007)
5. Figure 5. An overview of Sol-Gel Method with (a) colloidal sol film and (b) colloidal sol powder transformed into a gel
6. Figure 6. Measurement of pH level of ZnO nanofluid using electronic pH probe
7. Figure 7. pH strips are used to further verify the values obtained from electronic pH probe
8. Figure 8. Measurement of TiO_2 mass required for 0.05 vol% nanofluid preparation
9. Figure 9. Friction Losses in Pipes and Fittings Apparatus manufactured by Cussons Technology
10. Figure 10. Mechanical hand mixer is used to mix the nanofluids evenly to prevent agglomeration
11. Figure 11. Adjustment of flowrate using flowmeter
12. Figure 12. Head loss measurement using manometer
13. Figure 13. Flow Chart of Research Methodology
14. Figure 14. Project Activities Flow Chart
15. Figure 15. Key milestones for FYP I
16. Figure 16. Key milestones for FYP II

17. Figure 17. Curve of Fluid Friction Factor against Reynolds Number, Re at pipe diameter = 0.0235 m
18. Figure 18. Curve of Fluid Friction Factor against Reynolds Number, Re at pipe diameter 0.0133 m
19. Figure 19. Curve of Fluid Friction Factor against Reynolds Number, Re at pipe diameter 0.0085 m
20. Figure 20. Curve of theoretical and experimental fluid friction factor against Reynolds number for water
21. Figure 21. Curve of Fluid Friction Factor against Reynolds Number, Re at pipe diameter 0.0235 m
22. Figure 22. Curve of Fluid Friction Factor against Reynolds Number, Re at pipe diameter 0.0133 m
23. Figure 23. Curve of Fluid Friction Factor against Reynolds Number, Re at pipe diameter 0.0085 m

LIST OF TABLES

1. Table 1. Project Gantt Chart for Final Year Project I
2. Table 2. Project Gantt Chart for Final Year Project II
3. Table 3. Table of baseline data for fluid flow experiment for pipe diameter 23.5 mm
4. Table 4. Table of baseline data for fluid flow experiment for pipe diameter 13.3 mm
5. Table 5. Table of baseline data for fluid flow experiment for pipe diameter 8.5 mm
6. Table 6. Table of overall Reynolds number of all pipe diameter against theoretical fluid friction factor and experimental fluid friction factor
7. Table 7. Table of baseline data for fluid flow experiment for pipe diameter 23.5 mm
8. Table 8. Table of baseline data for fluid flow experiment for pipe diameter 13.3 mm
9. Table 9. Table of baseline data for fluid flow experiment for pipe diameter 8.5 mm

ABSTRACT

Nanofluids are explained as suspensions of nanoparticles in conventional heat transfer fluids. Nanofluids possess enhanced thermal conductivity therefore making it desirable for advanced heat transfer applications. Until recently, numerous studies and researches regarding nanofluids are directed towards heat transfer. Therefore, little is known regarding the relationship between nanofluids and how they affect fluid friction factor for flow in pipes. Hence, this study aims to study and determine the parameters responsible for affecting the fluid friction factor in pipes concerning nanofluids. The objectives of this study include studying preparation methods of nanofluids and also to determine the fluid friction factor for three nanofluids at the same concentration. The scope of the study focuses on oxide ceramics and metallic nanoparticles of different densities and viscosity. Firstly, a theory is developed to model the experiment and hence the outcome of the experiment can be predicted whereby fluid friction factor of different nanofluids is dependent on their respective densities. Secondly, nanoparticles dispersed in aqueous solutions are procured and nanofluids are synthesized by dilution with distilled water. The nanofluids are flowed into experimental pipe setup where their respective pressure drops are measured. Further data analysis is conducted to establish and evaluate the fluid friction factor by means of a Moody chart and Colebrook equation. The variable concerned in this study is the density of individual nanoparticles chosen.

CHAPTER 1

INTRODUCTION

1.1 Background of study

In this study, nanofluids; which are uniform and stable suspensions or dispersions of nanoparticles in base fluids (Choi, 1995) are introduced into distilled water. This suspension is then flowed into pipes and then is studied and analyzed in order to come up with its fluid friction factor. Different types of nanofluids of different densities are tested to determine the relationship between different densities and their respective friction factor. Certain procedures are followed in order to prepare the nanofluids prior to testing.

According to a presentation by Kostic (n.d.), nanofluids are a new breed of heat transfer fluids whereby nanoparticles of smaller than 100 nm are dispersed in conventional heat transfer fluids. Different nanoparticles of different densities are considered for usage. The types of nanoparticles chosen for the experiments include Silicon dioxide (SiO_2), Titanium dioxide (TiO_2), and Zinc dioxide (ZnO).

In 1845, Weisbach presented the fluid friction factor f as an empirical friction parameter which is a constituent of Darcy-Weisbach equation to describe pressure difference between 2 locations in a pipe (Munson et al., 2010). This pressure difference, or *head loss* is represented as

$$\Delta p = f \left(\frac{\ell}{D} \right) \left(\frac{V^2}{2g} \right)$$

Whereby f denotes fluid friction factor or Darcy friction factor, ℓ is the characteristic length of the pipe, D is the pipe diameter, V is fluid velocity and g is gravitational acceleration. Another less popular friction factor is Fanning friction factor which is simply $f/4$ which means that its value is a quarter than that of Darcy's.

In a fully developed laminar flow, the fluid friction factor f is yielded from the simple equation of

$$f = \frac{64}{Re}$$

Whereby Re denotes the Reynolds number dimensionless quantity. For fully developed turbulent flow, the determination of fluid friction factor is much more intricate since it is not identifiable via a clear theoretical analysis. Therefore, extensive experiments conducted by Nikuradse (1993) using artificially roughened pipes led to the establishment of the relation

$$\frac{1}{\sqrt{f}} = 2 \log(Re\sqrt{f}) - 0.8$$

The above mentioned equation is the base for the turbulent smooth flow portion of the Moody Chart developed by C.F Colebrook and L.F. Moody to establish a graphical curve-fitting to determine f in relation to Re and surface roughness.

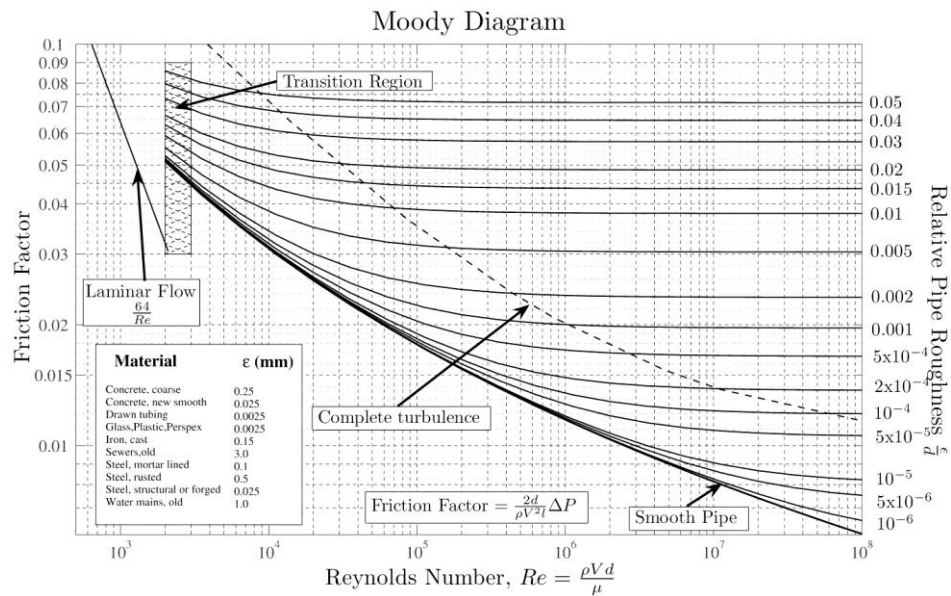


Figure 1. Moody Chart or Moody Diagram

(Retrieved from

http://upload.wikimedia.org/wikipedia/commons/8/80/Moody_diagram.jpg)

In this study, the fluid friction f of different flowrates are determined by measuring the pressure difference between two points in a pipe. This value is then incorporated into the Darcy-Weisbach equation to determine the fluid friction factor f . Using moody Chart, the relative surface roughness of pipes and Reynolds number is also used to pinpoint the fluid friction factor. The Reynolds number given by formula

$$Re = \frac{\rho V D}{\mu}$$

Where ρ denotes density of the fluid, V is the velocity of the fluid, D is the travelled length of the fluid, or the length of the pipe used in the experiment, and μ is the dynamic viscosity of the fluid.

1.2 Problem statement

The fluid friction factors for single phase fluids are already widely established. However, little is known regarding how suspensions of nanoparticles in fluids behave and how they affect the fluid friction factor in pipes. Therefore, this study aims to determine the parameters which are responsible in affecting the fluid friction factor of nanoparticles in pipes by experimenting with three different nanofluids with different densities which are Silicon dioxide (SiO_2), Titanium dioxide (TiO_2), and Zinc Oxide (ZnO) with densities of 2220 kg/m^3 , 4175 kg/m^3 and 5600 kg/m^3 respectively (Appendix).

1.3 Objectives of study

The main aim of this study is to determine the parameters which affect the fluid friction factors in pipes for nanofluids. This is achieved by experimenting with different types of nanofluids at constant concentrations.

The main objectives of the study include:

1. To study the preparation methodology of nanofluids
2. To determine the friction factor for three nanofluids at a constant concentrations

1.4 Scope of study

The scope of the study is directed towards the investigation of the fluid friction factor for oxide ceramics and metallic nanoparticles suspensions. Oxide ceramics as well as metal oxides such as SiO₂, TiO₂, and ZnO are commonly produced and obtained in powder form (Yu et al., 2007). In the form of powder, nanoparticles are dispersed throughout aqueous or organic base liquid to become nanofluids. Nanoparticles dispersed in H₂O (water) as the base fluid is readily available and are procured. This solution is then diluted with distilled water to achieve constant volume concentration of 0.05 vol %. The nanofluids are then flowed into experimental pipe setup so that the fluid properties can be analyzed and interpreted. This study focuses on obtaining the pressure difference between two points in the pipe so that the fluid friction factor can be determined.

CHAPTER 2

LITERATURE REVIEW

2.1 Introduction to nanofluids

According to Yu et al. (2007) Nanofluids are defined as nanotechnology-based heat transfer fluids derived by stably suspending nanometer-sized particles with typical lengths ranging from 1 to 100 nm (nanometers) in conventional heat transfer fluids most common in the form of liquids. The name “Nanofluid” was coined by Argonne National Laboratory and throughout research by nanofluid research groups worldwide, it is found that nanofluids have different thermal properties from conventional heat transfer fluids. In one of the studies, it is found that an addition of less than 1 % volume of nanoparticles to conventional heat transfer liquids has increased the thermal conductivity by 200 % (Choi et al., 2001). This phenomena is explained by Choi (1998) that since at room temperature, metals in solid phase possess higher thermal conductivity in fluids. For instance, thermal conductivity of copper at room temperature is 700 times higher than water and 3000 times higher than engine oil. Hence, the thermal conductivity of metallic fluids is found to be higher than non-metallic fluids thus increasing heat transfer ability.

As explained by Das et al. (2008), this discovery has led to numerous breakthroughs not only limited to enhancement of thermal properties of nanofluids, but also in proposing new mechanisms behind enhanced thermal properties of nanofluids, and development of new coolants such as smart coolants for computers and safe coolants for nuclear reactors.

2.2 Fabrication of nanoparticles and nanofluids

Yu et al. (2007) stated that nanoparticles possess unique physical and chemical properties as compared to larger particles of the same material. It is also explained that the nanoparticles are fabricated by either physical process or chemical process. In physical process, nanoparticles are either produced through mechanical grinding method or inert-gas-condensation method developed by Granqvist and Buhrman in 1976. On the other hand, in the chemical process, nanoparticles are produced through chemical precipitation, chemical vapor deposition, micro-emulsions, spray pyrolysis, and thermal spraying.

The synthesis of nanofluids also consisted of two techniques, which are two-step technique and single step technique. In a two-step technique, nanoparticles produced either by physical or chemical processes are dispersed in a base fluid. In a single step technique, nanoparticles are simultaneously produced and dispersed in base fluid.

Each technique has its own advantages and disadvantages. In a two-step process, the advantage includes production of nanoparticle powders in bulk are economically friendly by utilizing the inert gas condensation method (Romano et al. 1997). However, it is rendered impractical until the agglomeration problem is solved; whereby individual particles are quick to agglomerate prior to complete dispersion. This can be attributed to attractive Van Der Waals forces between nanoparticles. This issue needs to be tackled since one of the important factor in achieving success in heat transfer of nanofluids depends on the dispersion of monodispersed or non-agglomerated nanoparticles in liquids.

Single step process is most commonly used to synthesize nanofluids containing high-conductivity metals. This is to prevent oxidization of the particles. The uniqueness of this process lies in the way how the nanoparticles are produced and dispersed in a single process. Argonne National Laboratory (ANL) has patented this single step process in order to produce non-agglomerating copper nanoparticles dispersed uniformly in ethylene glycol. In this technique, nanophase powders are condensed directly from vapor phase and flowed into a flowing low-vapor-pressure ethylene glycol in a vacuum chamber. In another one step method, Chang et al. (2005) used submerged arc nanoparticle synthesis to produce nanofluids containing TiO_2 , Cu and CuO. Nanoparticles are produced by heating solid material from an electrode by arc sparking, after that it is condensed into liquid in a vacuum chamber to form nanofluid. In a commercial sense, the one step process is difficult for widespread use because it is expensive to operate and the usage of vacuum limits the rate of production of nanoparticles and nanofluids.

Besides the processes mentioned previously, there are quite a few alternatives in producing nanofluids depending on the combination of nanoparticle material and fluid (Yu et al., 2007). Among them include templating, electrolysis metal deposition, layer-by-layer assembly, microdroplet drying, and other colloid chemistry techniques.

2.3 Applications of nanofluids

De Leon & Wong (n.d.) explained that since nanofluids enhance thermo-physical properties which include thermal conductivity, thermal diffusivity, viscosity and convective heat transfer coefficients, they can be fully utilized in certain applications such as industrial cooling, transportations, electronics, nuclear reactors, biomedicine, and food.

In industrial cooling applications, a recent project conducted by Routbort et al. in 2008 by incorporating nanofluids for industrial cooling has yielded in less energy consumption and reduction in emissions. The potential of nanofluids as the replacement for cooling and heating water in the United States industry might save 1 trillion Btu of

energy. Moreover, in United States electric industry, 10 to 30 trillion Btu can be conserved annually by adapting closed-loop cooling cycles using nanofluids.

In terms of automotive applications, nanofluids have the potential of replacing the conventional coolant due to its increased thermal conductivity and higher efficiency. De Leon & Wong elaborated further that at high speeds, 65% of the energy output of trucks is used to overcome wind resistance. This issue is often blamed on the lack of aero dynamicity of the bulky front portion of trucks which houses large radiator grills aiming to optimize large surface area of air for cooling. Singh et al. (2006) has found that usage of nanofluids in radiators reduce frontal area by 10% and thus lead to fuel savings by 5%.

Nanofluids have made an impact in the electronics sector by its usage to cool microchips. Development of smaller microchips has often been limited by rapid heat dissipation. With the utilization of nanofluids as a medium for liquid cooling of computer processes, it is expected that while combining nanofluid oscillating heat pipes with thin film evaporation, the system will be able to remove heat fluxes over 10 MW/m² (Ma et al. 2006).

Advancements in biomedical industry have also capitalized on nanofluids in terms of drug delivery system. One initiative involves the usage of iron-based nanoparticles as delivery vehicles for drugs or radiation for cancer patients. Magnetic nanofluids are used to navigate particles through the bloodstream towards a tumor with magnets. Its key benefit is that it allows medical practitioners to apply high dosage of drugs or radiation on a local area without damaging nearby healthy tissues as often experienced in conventional treatment methods.

2.4 Previous related studies on nanoparticle friction factor

(Ko, et al., 2007) has conducted investigations on flow characteristics for aqueous suspensions of multi-walled carbon nanotubes (CNT). In preparing the nanotubes suspensions, they have utilized two different methods; the first being to disperse nanotubes by means of a surfactant and the other by using acid treatment to introduce oxygen-containing functional groups on the CNTs. The aim for their study is to investigate the pressure drops of CNT suspensions in horizontal tubes and measuring viscosity variation for different shear rates. The objective is to study the effect of CNT loading and preparation methods.

They prepared the nanofluids by using multi-walled CNTs and Distilled water (DW). The CNTs are obtained from external manufacturer and were produced by chemical vapour deposition. Since CNTs are hydrophobic in nature which raises concerns regarding agglomeration and precipitation in water, they have used sodium dodecyl sulfate (SDS) as a surfactant. 1 wt% of SDS was dissolved in DW followed by sonication of SDS and CNT solution to ensure well dispersed and homogeneous suspensions. The other method is by attaching hydrophilic functional group onto CNT surfaces by using nitric/sulfuric acid mixtures. By sequence, they first prepare 1 g of CNTs along with 40 ml acid mixture to be boiled and refluxed for the duration of 1 hour. Cleaned CNTs are collected and dried at 150 °C to remove any traces of water attached to it. The CNTs are considered treated and are mixed with DW in a mixing chamber. This mixture is then undergoes sonication. Ko et al. (2007) has highlighted that CNT nanofluids prepared using surfactant are termed as Pristine CNT nanofluids (PCNT) and its counterpart is referred to as Treated CNT nanofluids (TCNT).

To measure viscosity, they used a viscometer done on different CNT concentrations at shear rates ranging between 0.01 to 100 s⁻¹. To provide pumping power for fluid flow, they used a magnetic chemical pump, of which its pumping power was controlled by a digital inverter. They have used a stainless-steel tube with a length of 4 meters and inner diameter of 10.7 mm. The pressure drop is measured across 2 meters of piping using differential pressure transducers. The schematic of the pressure drop apparatus is illustrated below in figure 2.

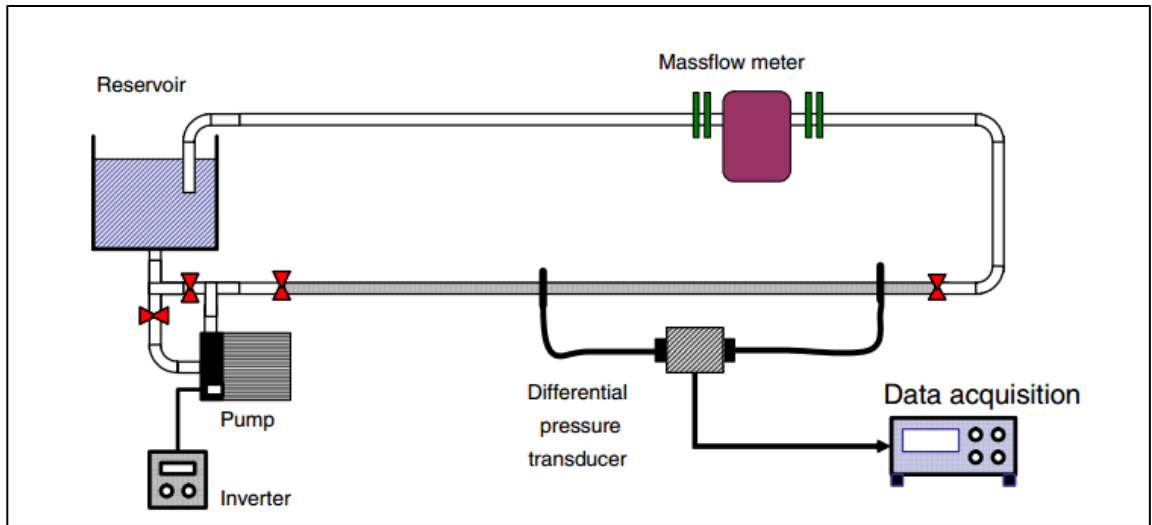


Figure 2. Schematic diagram of experimental apparatus to measure pressure drop as used by Ko et al. (2007)

The resulting pressure drop is analyzed and derived to find the fluid friction factor by using Darcy-Weisbach equation, and for baseline data of DW friction factor, they have utilized $f = 64/Re$ for laminar flow and Colebrook equation for turbulent flow as discussed in previous sections.

Figure 3 below shows a comparison of pressure drop between PCNT and TCNT nanofluids with 1400 ppm with DW in the horizontal tube. It is found that at low flow rates, PCNT undergoes a relatively larger pressure drop as compared to TCNT and DW. Ko et al. reasoned that this trend is governed by the small rise in viscosity for TCNT as compared to PCNT at similar volume fraction and shear rate. With the increase of flowrates however, the pressure drop trend of nanofluids becomes similar with DW. It is explained that as viscosity of nanofluids decreases with increasing shear rate, and hence pressure drop gap between the nanofluids and DW decreases.

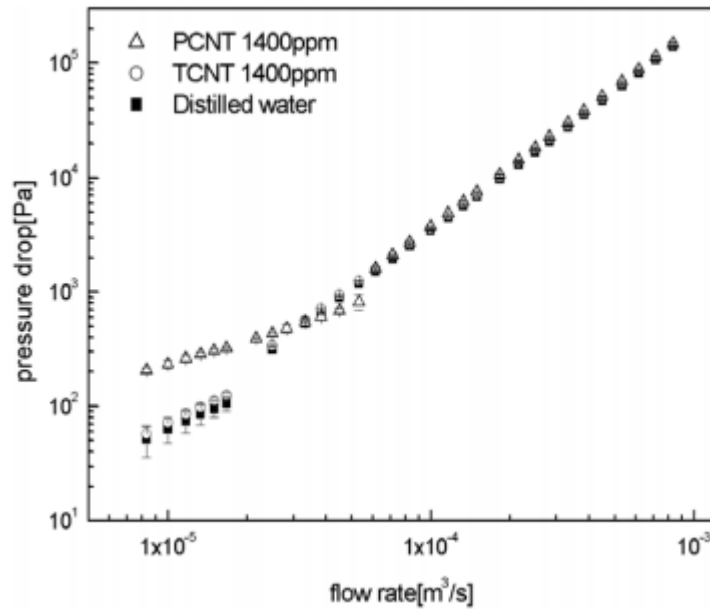


Figure 3. A graph of pressure drop (Pa) against flowrate (m^3/s) for DW, PCNT and TCNT for 1400 ppm CNT loading (Ko et al., 2007)

Figure 4 shows the relationship between fluid friction factor of TCNT, PCNT, and DW as a function of dimensionless value of Reynolds number. As expected, the trend for DW follows closely that of Newtonian fluids which verifies the experimental setup used. TCNT shows an initial increase in friction factor in laminar flow, in turbulent flow however, friction factor is similar with DW. In contrast, PCNT shows a substantial divergence from the DW trend in laminar flow as depicted in figure 4 a. It is observed that PCNT friction factor at laminar region is approximately 2.7 time than that of its TCNT counterpart. This trend is again attributed to the notable elevation of viscosity for PCNT. This data ultimately suggests that PCNT heat transfer systems may experience reduction in overall efficiency due to increase in friction drag. At turbulent flow region however, both PCNT and TCNT shows similar trend with DW. The reason being is that viscosity of PCNT increases decreases at high shear rate because of its shear thinning property.

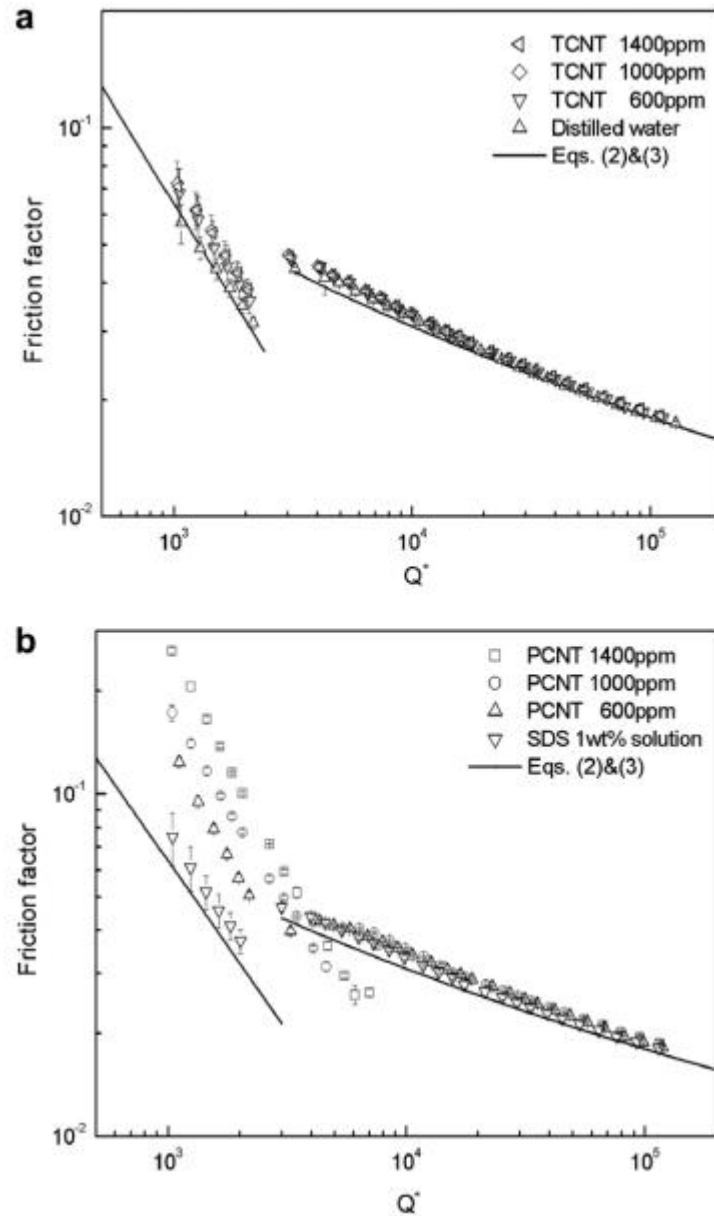


Figure 4. Graphs of friction factor against dimensionless flowrate/Reynolds number for DW as baseline for PCNT and TCNT (Ko et al., 2007)

Their study has come to the conclusion that both PCNT and TCNT possess shear thinning properties and this effect is most apparent on PCNT where at low shear rates, increase in viscosity is higher as compared to TCNT thus resulting in larger pressure drops in laminar flow condition.

2.5 Nanoparticles chosen for experimentation

2.5.1 Silicon Dioxide

Silicon dioxide, also known as silica is one of the most abundant compounds found on this planet (Uses/Acquirement of Silicon Dioxide, n.d). It is found naturally in the form of quartz and it can be observed in various living organisms (Iler, 1979). It is very hard, and has a relatively high melting and boiling temperature of 1610 °C and 2230 °C respectively. Silicon dioxide is extracted by mining and further purification of the mineral and contributes at least one tenth of the earth crust composition (Flörke et. al, 2008). It can be produced synthetically by quartz processing.

Silicon dioxide has a large contribution in modern electronics. One of them includes its usage in microchips. It is formed spontaneously on silicon wafers by means of thermal oxidation coined as native oxide with thickness of 1 nm (Doering, Robert and Nishi, 2007). This layer of native oxide act as insulators with high chemical stability and its benefits extend to protecting the silicon wafers, current blockage and limits current flow (Riordan, 2007). Aside from insulation, Silicon dioxide is piezoelectric; which means that it is able to convert mechanical energy to electric energy and vice versa. This allows it to transmit and receive radio signals (Uses/Acquirement of Silicon Dioxide, n.d).

In terms of nanotechnology, silica nanoparticles in the form of silica aerogels are known as one of the best thermal insulators (Silica Nanoparticles, n.d.). It comprises of silica nanoparticles interspersed with nanopores containing air. By taking advantage of the low thermal conductivities of both air and silica it makes for a great heat insulator. Furthermore, in biomedical industry, silica nanoparticles are studied for its usefulness to deliver drugs by optimizing its pores to store therapeutic molecules.

2.5.2 Titanium Dioxide

Titanium oxide is a naturally occurring oxide of titanium and is found in the form of rutile, anatase and brookite minerals. The most common source of titanium oxide is ilmenite ore followed by rutile which contains 98% of titanium dioxide. By heating anatase and brookite phases in the range of 600 °C to 800 °C, they convert irreversibly to equilibrium rutile phase (Greenwood and Earnshaw, 1984).

Titanium Dioxide is most commonly used as white pigment due to its high UV resistance and diffraction index along with solid light scattering ability. Thus, it is used in white dispersion paints, varnishes, dyes, and textiles. It is also used in toothpaste and drug as food additive (Titanium Dioxide-Material Information, n.d.).

By contrast, nanoscale Titanium Dioxide is not used as food additive, but is optimized in wood preservatives, textile fibers, and high-factor sun protection creams (Weir, Westerhoff, Fabricius & Van Goetz, 2012). Presently, nanoscale titanium oxide has contributed towards the achievement of high sun protection factors (Sicherheit von Nanopartikeln in Sonnenschutzmitteln, 2010). However, nanoscale Titanium Dioxide production volume amounts to only 1 % of the production volume of Titanium Dioxide pigments mentioned previously.

2.5.3 Zinc Oxide

Zinc oxide occurs in the form of white powder (Klingshirn, 2007). In crystalline form, Zinc Oxide is thermochromic, and changes in colour from white to yellow upon heating and reverting to original white colour upon cooling (Wilberg & Holleman, 2001). It is insoluble in water but is soluble in acids (Greenwood & Earnshaw, 1997). According to Porter (1991), there are three main processes of producing Zinc Oxides which are; indirect process, direct process and wet chemical process.

In indirect process, Zinc metal in graphite crucible is melted and vaporized at high temperatures around 1000 °C. As a product, Zinc vapours react with Oxygen to form Zinc Oxide along with a decrease in temperature and high luminosity. The produced particles then enter a cooling vent and are gathered afterwards. By contrast, the direct process begins with zinc ores or contaminated zinc composites. They are in turn reduced via carbothermal reduction, whereby the zinc ores are heated alongside anthracite to yield zinc vapour. From here, the direct process develops in a way similar to indirect process in which Zinc vapour are oxidized. Due to low purity of zinc ores used as source material, Zinc Oxides produced are of lower quality than the indirect process. In wet chemical process, Zinc carbonate or Zinc hydroxides suspended in aqueous solutions is precipitated, washed, dried and calcined.

Kołodziejczak-Radzimska and Jesionowski (2014) states that production of Zinc Oxides by Sol-Gel method draws attention due to its straightforward, cheap, reliable, high repeatability and mild condition of synthesis. Figure below shows an overview of two instances of Zinc Oxide synthesis by using Sol-Gel method.

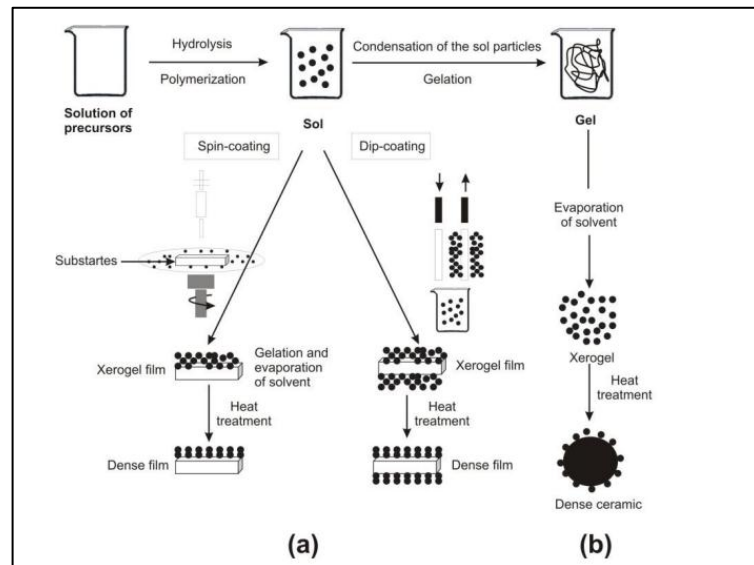


Figure 5. An overview of Sol-Gel Method with (a) colloidal sol film and (b) colloidal sol powder transformed into a gel

The aforementioned qualities of Sol-Gel method have enabled surface modification of Zinc Oxide with selected organic compounds. By means of X-Ray Diffraction (XRD), Scanning Electron Microscopy (SEM), nitrogen adsorption isotherms and UV-Vis spectroscopy, Benhebal et al. (2013) has discovered a hexagonal wurtzite structure with spherically shaped particles as a result of Sol-Gel preparation method from Zinc Acetate Dihydrate, oxalic acid, and ethanol as solvent.

Among its application includes the rubber industry, where it is used to produce an array of cross-linked rubber products (Das et al., 2011). In silicone rubber, the thermal conductivity is low, and is therefore enhanced by utilizing thermal conductivity fillers such as metal oxides. These nano-scale fillers are able to deliver high thermal conductivity at relatively low filling content. However, there have been issues regarding Zinc Oxides nanoparticles as they tend to agglomerate together to form large size particles due to weak interaction between the polymer and the surface of the nanoparticles. To overcome this predicament, Yuan et al. (2011) proposed surface-modified Zinc Oxide nanoparticles with vinyl silane group to be fused into silicon rubber by hydrosilylation reaction during curing. It is found that mechanical properties and thermal conductivity increases due to better cross-linkage between Zinc Oxide and silicon rubber matrix.

CHAPTER 3

RESEARCH METHODOLOGIES AND PROJECT ACTIVITIES

2.1 Research methodology

Selection of nanoparticles and base fluid

In this study, three types of nanoparticles are to be considered based on their densities before they are suspended in the base fluid. The nanoparticles shortlisted are Silicon dioxide (SiO_2) with density of 2220 kg/m^3 , Titanium dioxide (TiO_2) with density of 4175 kg/m^3 , and Zinc Oxide (ZnO) with density of 5600 kg/m^3 (Appendix). It is worth to note the mentioned densities for the nanoparticles are theoretical values and that to ensure the integrity of the experimental values are not compromised, the nanoparticles are to be manually weighed and measured prior to the dilution of nanofluids with base solution. The particle sizes of each nanofluids vary, with SiO_2 particle sizes ranges between 5-35 nm, TiO_2 particle size of 5-30 nm, and ZnO particle size of 30-40 nm. The base fluid chosen is distilled water readily available in the laboratory.

Theoretical Modelling of Experiment

Prior to conducting the experiment, a theoretical model based on calculations is devised to predict the outcome of the experimental results. In doing so, several assumptions are made with the main argument that in incompressible flow, the nanoparticles suspended in the base fluid moves at the same dimensionless flowrate Reynolds number,

$$Re_{base\ fluid} = Re_{nanoparticles}$$
$$\left(\frac{\rho V D}{\mu}\right)_{base\ fluid\ (H_2O)} = \frac{\rho_{nanoparticle} V_{nanoparticle} D_{nanoparticle}}{\mu_{base\ fluid\ (H_2O)}}$$

This equation is made relevant to find out the actual velocity of a single nanoparticle travelling in the pipe. Once the velocity of the nanoparticle is determined, its fluid friction factor is determined by optimizing Darcy-Weisbach equation using the

theoretical head loss due to base fluid at the same Reynolds number. This value is then multiplied to the total number of nanoparticles at concentration of 0.05 vol % at any given instance for a 1 meter pipe with inner diameters of 23.5 mm, 13.3 mm, and 8.5 mm pipes. This value is then added to the theoretical friction factor of base fluid only obtained from moody chart.

Fluid friction factor for water as base fluid is determined by utilizing moody chart for a given Reynolds number which corresponds to the volumetric flowrate ranging from 0.4 to 1.8 m³/h. The curve selected in the moody chart would be smooth pipe curve since the fluid friction apparatus have a smooth pipe made from Polyvinyl Chloride (PVC).

Same procedure is repeated for different densities of different nanoparticles obtained from appendix. The curve of the fluid friction factors of different nanoparticles are formulated and compared. The modelling procedure and results would be discussed extensively in Chapter 4.

Nanofluids preparation

The nanofluids are first tested for its pH level by using electronic pH probe and pH test strips. For each type of nanofluid, a concentration of 0.05 vol% are concocted and used in order to study the effect of different densities at similar volumetric concentration towards fluid friction factor. To achieve this concentration, SiO₂ nanofluids originally of 25% weight percentage, TiO₂ nanofluids of 15% weight percentage, and ZnO nanofluids of 20% weight percentage are diluted with distilled water, and mixed using mechanical stirrer. The equation used to determine the volume of nanofluid needed to be added to 30 liters of water is Scherrer's Equation (Sundar, Farooky, Sarada & Singh, 2013),

$$Volume\ concentration, \varphi\ \% = \frac{\left(\frac{W}{\rho}\right)_{nano}}{\left(\frac{W}{\rho}\right)_{nano} + \left(\frac{W}{\rho}\right)_{base\ fluid}} \times 100$$



Figure 6. Measurement of pH level of ZnO nanofluid using electronic pH probe



Figure 7. pH strips are used to further verify the values obtained from electronic pH probe

Step-by-step calculations for determining the volume of nanoparticles are explained below to prepare 0.05 vol% TiO₂ nanofluid solution by diluting a 15 wt% TiO₂ aqueous dispersion,

$$1. \text{Vol \%} = \frac{V_{\text{nano}}}{V_{\text{nano}} + V_{\text{base}}} \times 100$$

$$2. 0.05 \% = \frac{V_{\text{nano}}}{V_{\text{nano}} + V_{\text{base}}} \times 100$$

$$3. 0.0005 = \frac{V_{\text{nano}}}{V_{\text{nano}} + V_{\text{base}}}$$

For $V_{\text{base}} = 30 \text{ liters}$,

$$4. 0.0005 = \frac{V_{\text{nano}}}{V_{\text{nano}} + 30 \text{ l}}$$

$$5. V_{\text{nano}} = 0.015 \text{ liters} = 0.000015 \text{ m}^3$$

$$6. \text{mass}_{\text{nano}} = \rho V = (0.000015 \text{ m}^3)(4175 \text{ kg/m}^3) = 0.062625 \text{ kg} = 62.6 \text{ g}$$

7. For 15 wt% TiO₂ dispersion,

$$\frac{62.6 \text{ g}}{x} = 15\% = 0.15$$

$$x = 417.33 \text{ g}$$

Therefore, 417.33 g of aqueous TiO₂ solution needs to be added to 30 liters of water to achieve 0.05 vol% solution. Aqueous TiO₂ solution to be added is measured using electronic balance as seen in figure 8 below.



Figure 8. Measurement of TiO₂ mass required for 0.05 vol% nanofluid preparation

Experimental procedures

Experiments are conducted using fluid friction apparatus setup as shown in figure 9 below. It is a self-contained water circulating unit as a trainer for study of friction losses in pipes, pipe fittings and valves. Basically, the unit consists of a pump, storage tank, and a panel where all friction loss components and measuring apparatus are placed.

The panel consists of a H₂O manometer which measures pressure drop in the form of head loss, flow control valve to regulate fluid flow, flowmeter to measure the fluid flowrate, and a pressure control valve. The pipes of which the experiments are to be run are horizontal pipes similar in length (1 m) but differing in diameter with each having 23.5 mm, 13.3 mm, and 8.5 mm inner diameters.

In the experiments, major head loss (Darcy-Weisbach equation) for straight pipes of different types and diameters are determined for different flowrates ranging from 0.4 m³/h to 2.0 m³/h.



Figure 9. Friction Losses in Pipes and Fittings Apparatus manufactured by Cussons Technology

The procedures for the experiment are explained as follows:

1. Apparatus set up

1. Fluid friction apparatus is flushed using distilled water to remove any excess/contaminants which may be left behind by previous users. Water is allowed to flow at $1.8 \text{ m}^3/\text{h}$ for 10 minutes.
2. Excess water in the fluid apparatus is left to drain from the pipes.
3. Once most/all water is drained from the pipes, air is purged through the pipes from the pressure release valve using compressed air. Air is allowed to purge through the pipes for 5 minutes.
4. The storage tank is rid of the flushing water and is allowed to dry/wiped clean.
5. 30 liters of distilled water is added into the storage tank of the fluid friction apparatus.
6. Measured nanofluid mass required for dilution is added into the storage tank.
7. The solution is mixed well using mechanical hand mixer as shown in figure 10 for 15 minutes.
8. The pump is turned on and all valves on the apparatus are allowed to open so that the nanofluids will be able to circulate through all channels.



Figure 10. Mechanical hand mixer is used to mix the nanofluids evenly to prevent agglomeration

2. Operation of Fluid Friction Apparatus

1. The pipe network is primed with water/nanofluid.
2. Pipe with diameter 8.5 mm is selected by closing other valves.
3. Flowrate is adjusted accordingly between 0.4, 0.6, 0.8, 1.0, 1.2, 1.4, and 1.8 m³/h using flowmeter.

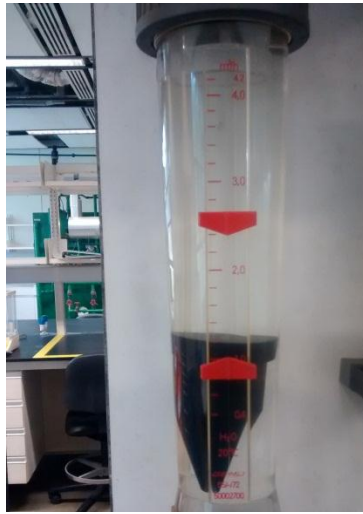


Figure 11. Adjustment of flowrate using flowmeter

4. Pressure loss at each flowrate instances is measured using H₂O manometer.

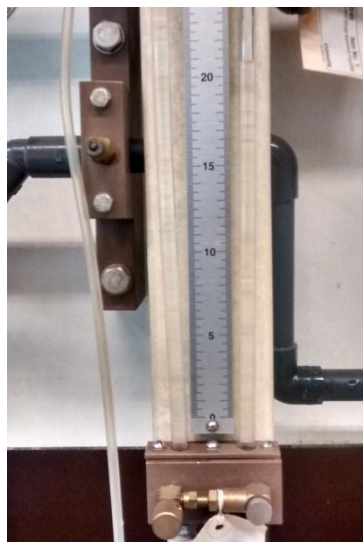


Figure 12. Head loss measurement using manometer

5. Procedure is repeated using different flowrates for pipe diameters 23.5 mm and 13.3 mm.
6. Fluid friction factor for water/nanofluid flow is obtained by solving Darcy equation for f ,

$$\Delta p = f \left(\frac{\ell}{D} \right) \left(\frac{V^2}{2g} \right)$$

Whereby,

Δp = Measured head loss using manometer (mmH₂O)

ℓ = 1 m (Characteristic length of the pipe)

D = 8.7 mm, 13.3 mm and 8.5 mm (Inner diameter of each pipe)

V = Velocity of water, derived from continuity equation, $Q = AV$

g = Gravitational acceleration, 9.81 m/s²

f = Fluid friction factor

Methodology Flow Chart

In short, the methodology for the study/research is as depicted below.

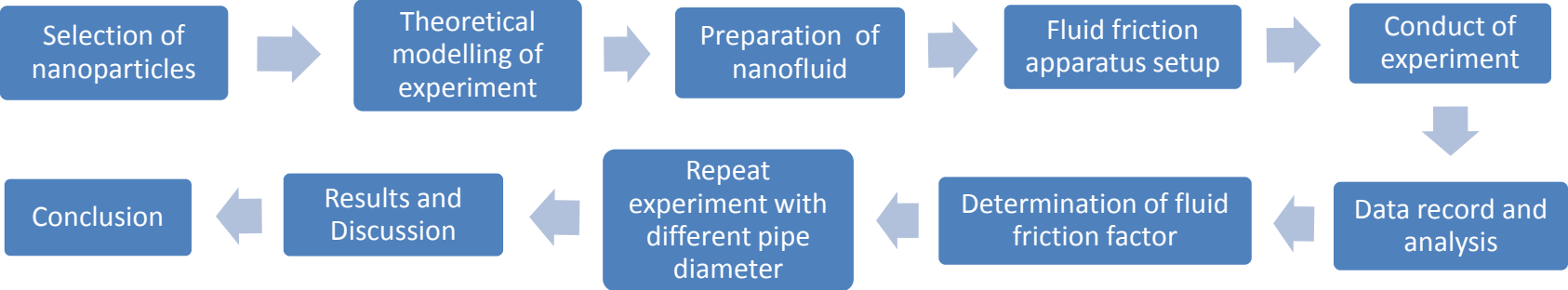


Figure 13. Flow Chart of Research Methodology

2.2 Project activities

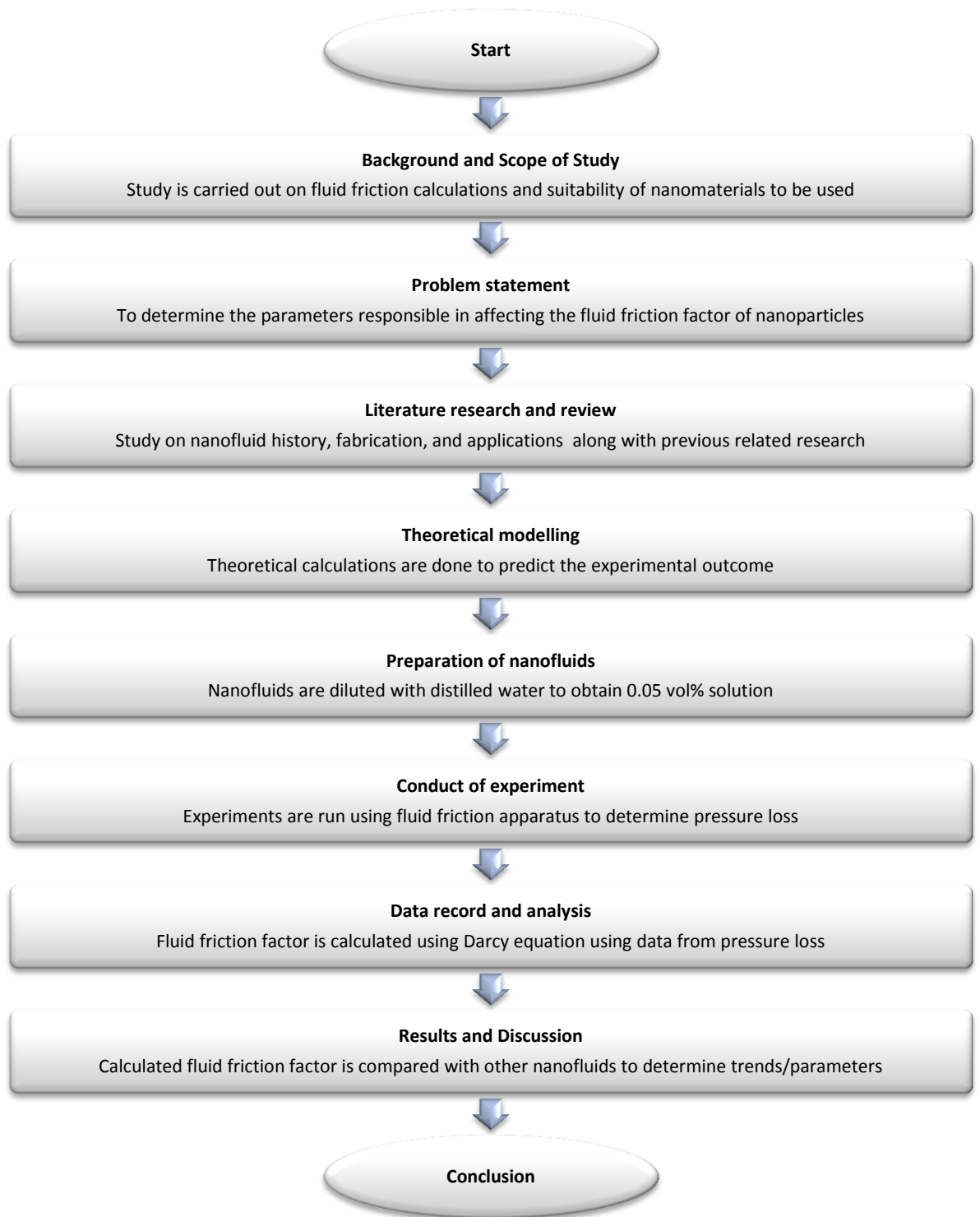


Figure 14. Project Activities Flow Chart

2.3 Research Gantt Chart

Table 1. Project Gantt Chart for Final Year Project I

MILESTONES	FYP I WEEK NUMBER													
	MAY		JUNE				JULY				AUGUST			
	1	2	3	4	5	6	7	8	9	10	11	12	13	14
Selection of Project Title	■	■	◆											
Preliminary Research Work				■										
Project planning				■	■									
Literature research and review					■	■								
Identification of experimental procedures					■	■								
Submission of Extended Proposal							■	■	◆					
Proposal Defense presentation										■	■	◆		
Continuation of project work											■	■	■	
Submission of Interim report draft													◆	
Submission of Interim report														◆

Table 2. Project Gantt Chart for Final Year Project II

MILESTONES	FYP II WEEK NUMBER													
	SEPTEMBER		OCTOBER				NOVEMBER				DECEMBER			
	1	2	3	4	5	6	7	8	9	10	11	12	13	14
Procurement and Order of Nanomaterials	■	■	■											
Preparation of Nanomaterials				■	◆									
Experiment on SiO ₂					■	■								
Experiment on ZnO						■								
Experiment on TiO ₂							■							
Preparation of Progress Report							■	■						
Submission of Progress Report								◆						
Troubleshoot and improvement									■					
Preparation for Pre-Sedex									■	■				
Pre-SEDEX										◆				
SEDEX											■	◆		
Preparation of Final Report												■	■	
Submission of Dissertation														◆
FYP II final presentation														◆

2.4 Research key milestones

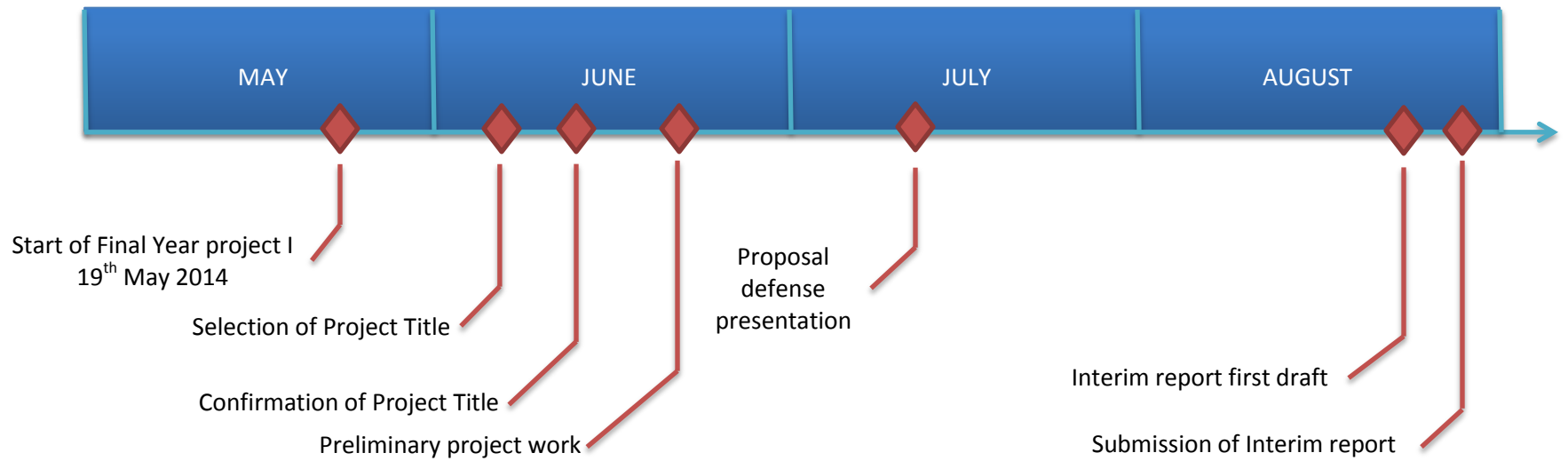


Figure 15. Key milestones for FYP I

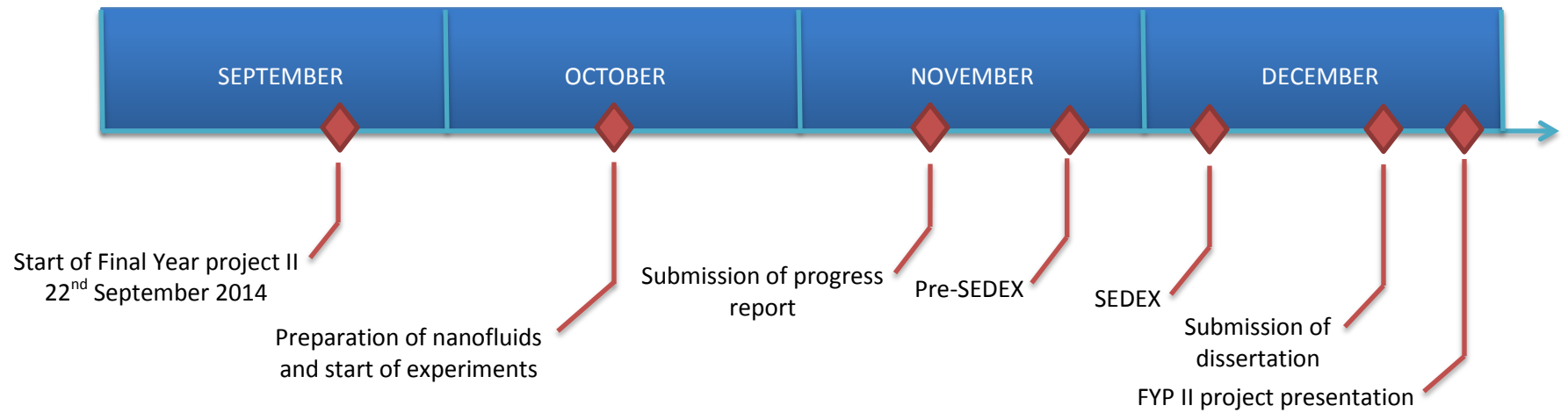


Figure 16. Key milestones for FYP II

CHAPTER 4

THEORETICAL MODELLING OF EXPERIMENT

4.1 Assumptions and Equations used for modelling

Prior to running the experiment, the results are predicted through a set of theoretical calculations aimed at predicting the outcome of the experiments. Various assumptions are taken into consideration in developing the model. Among the assumptions include:

1. Surrounding/working temperature is at 20 °C
2. Density of water is taken as 998.2 kg/m³
3. Dynamic/absolute viscosity of water is taken as 1.002 × 10⁻³ N.s/m²
4. All pipes through which nanofluid/baseline water is flowed are smooth pipes
5. In incompressible flow, the Re of water is the same as the Re of nanoparticle suspension

$$Re_{base\ fluid(H_2O)} = Re_{nanoparticles}$$
$$\left(\frac{\rho VD}{\mu}\right)_{base\ fluid\ (H_2O)} = \frac{(\rho VD)_{nanoparticles}}{\mu_{base\ fluid\ (H_2O)}}$$

6. Fluid friction factor for water is approximated using moody chart
7. Fluid friction factor due to presence of nanoparticles in a pipe section is the product of fluid friction factor of a single nanoparticle with the total number of particles in a pipe section of 1 meter in length for homogeneous aqueous nanofluid solution of 0.05 vol%.
8. Fluid friction factor of single nanoparticle is calculated from Darcy-Weisbach equation using pressure drop values due to baseline water.
9. The resultant friction factor would be the sum of the friction factor due to baseline water and presence of nanoparticles in pipe section.

All the assumptions mentioned previously are incorporated into a series of calculations aimed at reaching a logical explanation on the effect of nanoparticle density on fluid friction factor. Note that absolute viscosity of the nanofluid is assumed to be the same as baseline water since at very small concentration of 0.005 vol%, the viscous effects contributed by nanoparticles can be considered negligible.

4.2 Modelling procedures

The following procedures explain the steps taken in carrying out this simulation for flow through a pipe with diameter of 13.3 mm:

A. Determining fluid friction factor for baseline water

1. The data range for flowrate start from 1.0 m³/h with increments by 0.2 m³/h until 1.8 m³/h
2. The flowrate units are converted from m³/h to m³/s.
3. The average velocity of the fluid is calculated using continuity equation,

$$Q = AV$$

Whereby,

Q is the volumetric flowrate (m³/h)

A is the cross-sectional area of pipe (m²)

V is the average fluid velocity (m/s)

4. Reynolds number for baseline water is calculated using equation

$$\left(\frac{\rho V D}{\mu} \right)_{base\ fluid\ (H_2O)}$$

Whereby,

ρ is the density of water at 20 °C taken as 998.2 kg/m³

V is the calculated fluid velocity from continuity equation (m/s)

D is the hydraulic diameter of water taken as 13.3 mm/0.0133 m

μ is the dynamic viscosity of water at 20 °C taken as 1.002 × 10⁻³ N.s/m²

5. By using moody chart, the corresponding fluid friction factor for a given Reynolds number is approximated.
6. Pressure drop/head loss value at given reynolds number is evaluated using Darcy-Weisbach equation.

B. Determining fluid friction factor of nanoparticles

1. The volume of 1 meter pipe section with inner diameter of 13.3 mm is calculated by using equation

$$V_{cylinder} = \frac{\pi d^2}{4} \times l$$

Whereby,

d is the inner pipe diameter water taken as 13.3 mm/0.0133 m

l is the characteristic length of the pipe section taken as 1 m

2. For volume concentration of 0.05%, the volume fraction is multiplied by the volume of the pipe section to determine the total volume of all nanoparticles at any given instance in the pipe section.
3. By taking an average nanoparticle diameter of 30 nm, the volume for one nanoparticle is calculated by using equation

$$V_{nanoparticle} = \frac{\pi d^2}{4}$$

Whereby,

d is the diameter of a single nanoparticle taken as 3×10^{-8} m

4. Total volume of all nanoparticles is divided by the volume of a single nanoparticle to yield the total number of nanoparticles in the pipe section.
By taking into consideration that $Re_{base\ fluid(H_2O)} = Re_{nanoparticles}$, the average velocity of a single nanoparticle is determined.
5. Fluid friction factor of a single nanoparticle is calculated by substituting the velocity determined previously into Darcy-Weisbach equation for corresponding Reynolds number and pressure drop calculated in A.
6. Fluid friction factor due to single nanoparticle is multiplied with the total number of nanoparticles in pipe section to determine overall nanoparticle contribution to friction factor.
7. The value calculated previously is added with baseline water to yield resultant fluid friction factor of nanofluid.
8. Procedure is repeated for different nanoparticle type and pipe diameters.

4.3 Results

All calculations mentioned before are done with the aid of Microsoft Excel, and the graphs showing the curve of SiO₂, TiO₂, and ZnO nanofluids fluid friction factor against Reynolds number are as shown in figures 17, 18, and 19 for each diameter of 23.5 mm, 13.3 mm and 8.5 mm diameter pipes respectively.

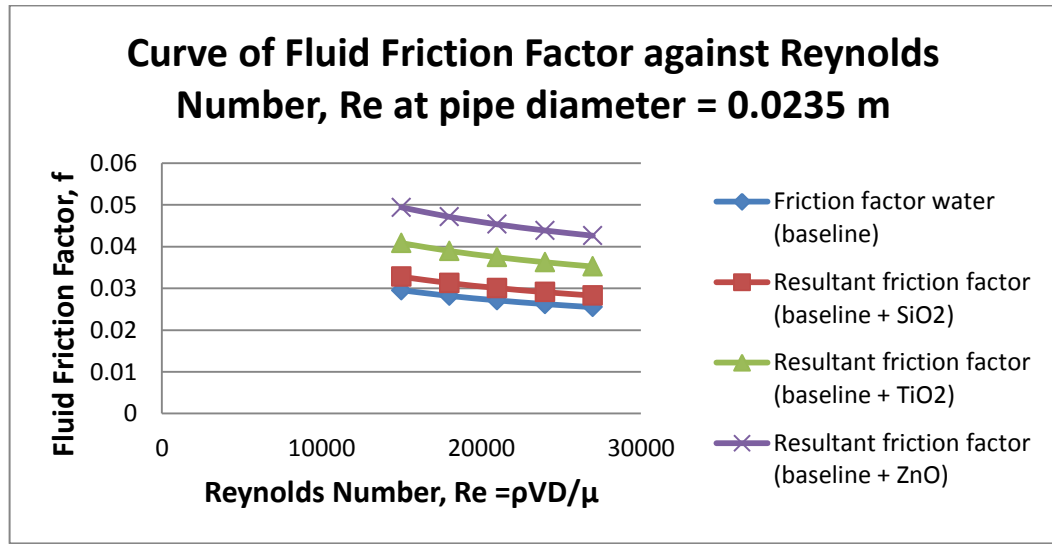


Figure 17. Curve of Fluid Friction Factor against Reynolds Number, Re at pipe diameter 0.0235 m

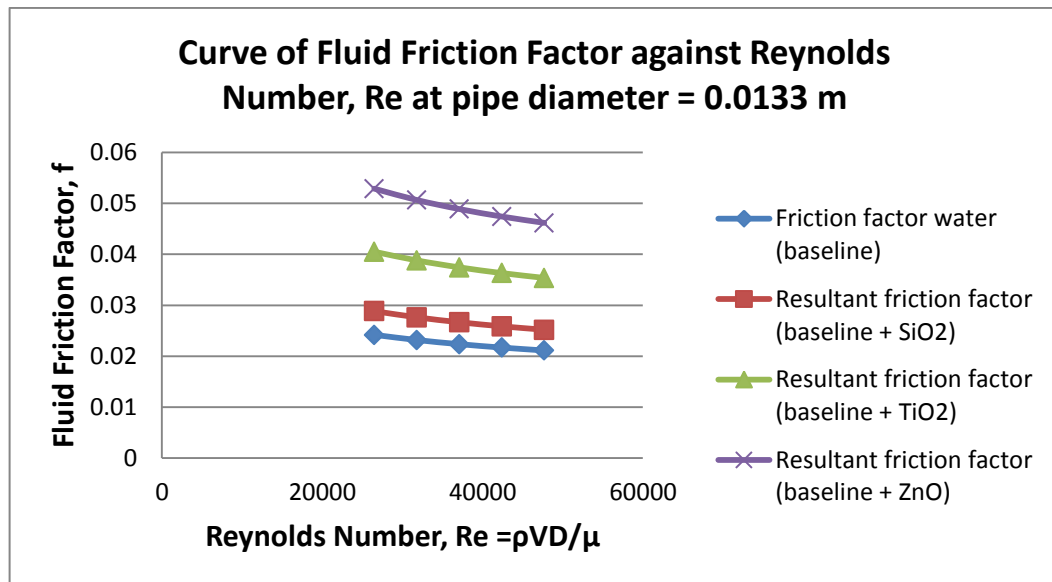


Figure 18. Curve of Fluid Friction Factor against Reynolds Number, Re at pipe diameter 0.0133 m

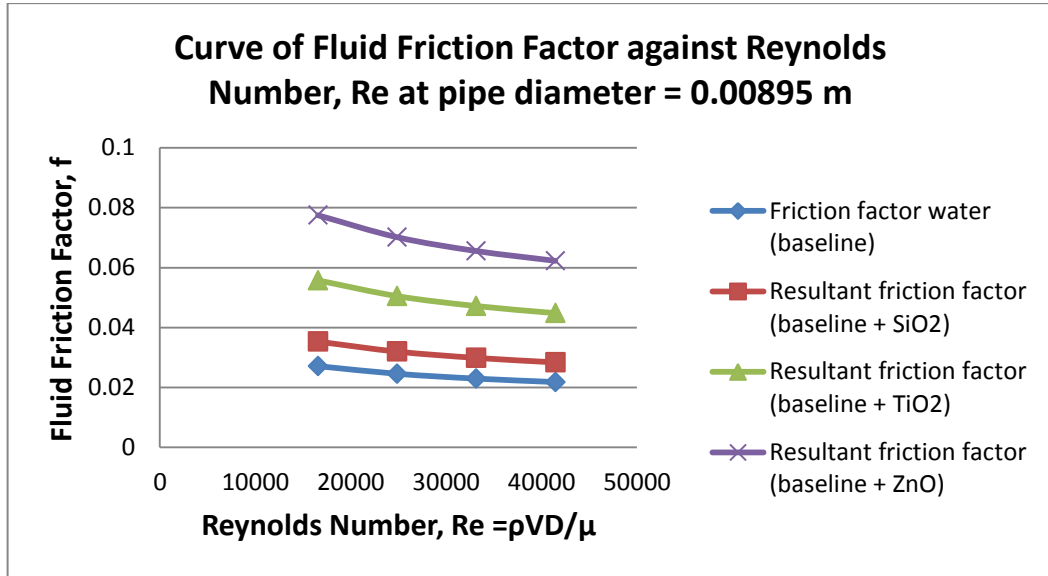


Figure 19. Curve of Fluid Friction Factor against Reynolds Number, Re at pipe diameter 0.0085 m

It can be observed that the trend shows that at turbulent flow, all nanofluids behave in a similar manner as water. It therefore proves that viscous effects of the nanoparticles in the aqueous dispersion is negligible and thus shear thinning effect as observed in PCNT and TCNT study by Ko et al., (2007) is not present.

Another pattern that emerges is the effect density of respective nanoparticles dictates the fluid friction factor. As density increases, fluid friction factor would also increase. It is attributed to the argument that by equating both Re of water and Re of nanoparticle while maintaining value for absolute/dynamic viscosity of water and nanoparticle size while varying nanoparticle density will yield an increase in velocity as the density of nanoparticles increases. Ultimately, the fluid friction factor calculated from Darcy-Weisbach equation would be larger due to larger velocity.

CHAPTER 5

EXPERIMENTAL RESULTS AND DISCUSSION

5.1 Results for baseline data (water)

A series of experiments are carried out to first find the fluid friction factor for water. This data serves as the baseline of which data for nanofluids are compared with. The experiments are carried out several times to find the average value for pressure drop. Data obtained are as displayed below.

Table 3. Table of baseline data for fluid flow experiment for pipe diameter 23.5 mm

Large diameter pipe (23.5 mm inner diameter)						
Flowrate (m ³ /h)	Pressure drop (mH ₂ O)	Characteristic length of pipe (m)	Hydraulic diameter (m)	Average velocity (m/s)	Gravitational acceleration (m/s ²)	Fluid friction factor, f
1.0	0.015	1	0.0235	0.6404	9.81	0.01666
1.2	0.020	1	0.0235	0.7685	9.81	0.01590
1.4	0.027	1	0.0235	0.8966	9.81	0.01529
1.6	0.034	1	0.0235	1.0247	9.81	0.01479
1.8	0.041	1	0.0235	1.1528	9.81	0.01437

Table 4. Table of baseline data for fluid flow experiment for pipe diameter 13.3 mm

Medium diameter pipe (13.3 mm inner diameter)						
Flowrate (m ³ /h)	Pressure drop (mH ₂ O)	Characteristic length of pipe (m)	Hydraulic diameter (m)	Average velocity (m/s)	Gravitational acceleration (m/s ²)	Fluid friction factor, f
1.0	0.127	1	0.0133	1.9994	9.81	0.00826
1.2	0.177	1	0.0133	2.3993	9.81	0.00802
1.4	0.229	1	0.0133	2.7992	9.81	0.00762
1.6	0.292	1	0.0133	3.1991	9.81	0.00745
1.8	0.358	1	0.0133	3.5990	9.81	0.00721

Table 5. Table of baseline data for fluid flow experiment for pipe diameter 8.5 mm

Small diameter pipe (8.5 mm inner diameter)						
Flowrate (m ³ /h)	Pressure drop (mH ₂ O)	Characteristic length of pipe (m)	Hydraulic diameter (m)	Average velocity (m/s)	Gravitational acceleration (m/s ²)	Fluid friction factor, f
0.4	0.190	1	0.0085	1.9581	9.81	0.00827
0.6	0.395	1	0.0085	2.9371	9.81	0.00763
0.8	0.652	1	0.0085	3.9162	9.81	0.00709
1.0	0.973	1	0.0085	4.8952	9.81	0.00677

Table 6. Table of overall Reynolds number of all pipe diameters against theoretical fluid friction factor and experimental fluid friction factor

Reynolds number	Fluid friction factor (theory)	Fluid friction factor (experimental)
14993.04	0.01666	0.02781
16580.53	0.00827	0.02711
17991.64	0.01590	0.02657
20990.25	0.01529	0.02558
23988.86	0.01479	0.02476
24870.80	0.00763	0.02455
26491.46	0.00826	0.02418
26987.47	0.01437	0.02408
31789.75	0.00802	0.02317
33161.07	0.00709	0.02294
37088.04	0.00762	0.02235
41451.34	0.00677	0.02179
42386.33	0.00745	0.02168
47684.62	0.00721	0.02111

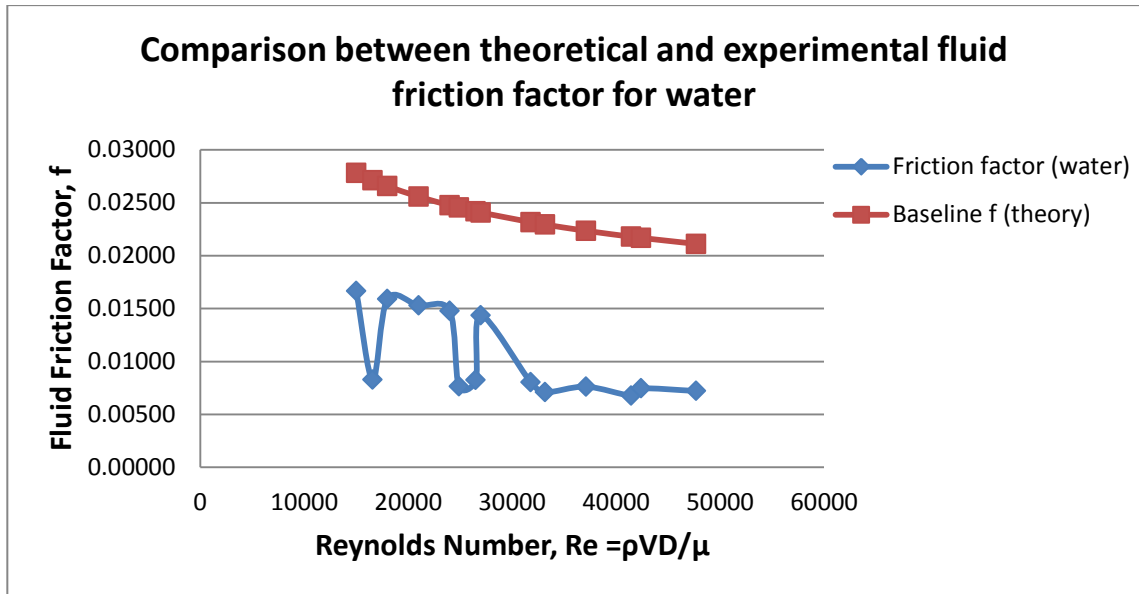


Figure 20. Curve of theoretical and experimental fluid friction factor against Reynolds number for water

5.2 Results for nanofluids

Table 7. Table of baseline data for fluid flow experiment for pipe diameter 23.5 mm

Large diameter pipe (23.5 mm inner diameter)						
Flowrate (m ³ /h)	Pressure drop (mH ₂ O)	Characteristic length of pipe (m)	Hydraulic diameter (m)	Average velocity (m/s)	Gravitational acceleration (m/s ²)	Fluid friction factor, f
For SiO₂ nanofluids of 0.05 vol% concentration						
1.0	0.019	1	0.0235	0.6404	9.81	0.02098
1.2	0.023	1	0.0235	0.7685	9.81	0.01796
1.4	0.031	1	0.0235	0.8966	9.81	0.01778
1.6	0.039	1	0.0235	1.0247	9.81	0.01713
1.8	0.047	1	0.0235	1.1528	9.81	0.01619
For TiO₂ nanofluids of 0.05 vol% concentration						
1.0	0.030	1	0.0235	0.6404	9.81	0.03335
1.2	0.040	1	0.0235	0.7685	9.81	0.03149
1.4	0.052	1	0.0235	0.8966	9.81	0.03002
1.6	0.061	1	0.0235	1.0247	9.81	0.02664
1.8	0.070	1	0.0235	1.1528	9.81	0.02417
For ZnO nanofluids of 0.05 vol% concentration						
1.0	0.038	1	0.0235	0.6404	9.81	0.04287
1.2	0.052	1	0.0235	0.7685	9.81	0.04065
1.4	0.068	1	0.0235	0.8966	9.81	0.03888
1.6	0.084	1	0.0235	1.0247	9.81	0.03708
1.8	0.106	1	0.0235	1.1528	9.81	0.03668

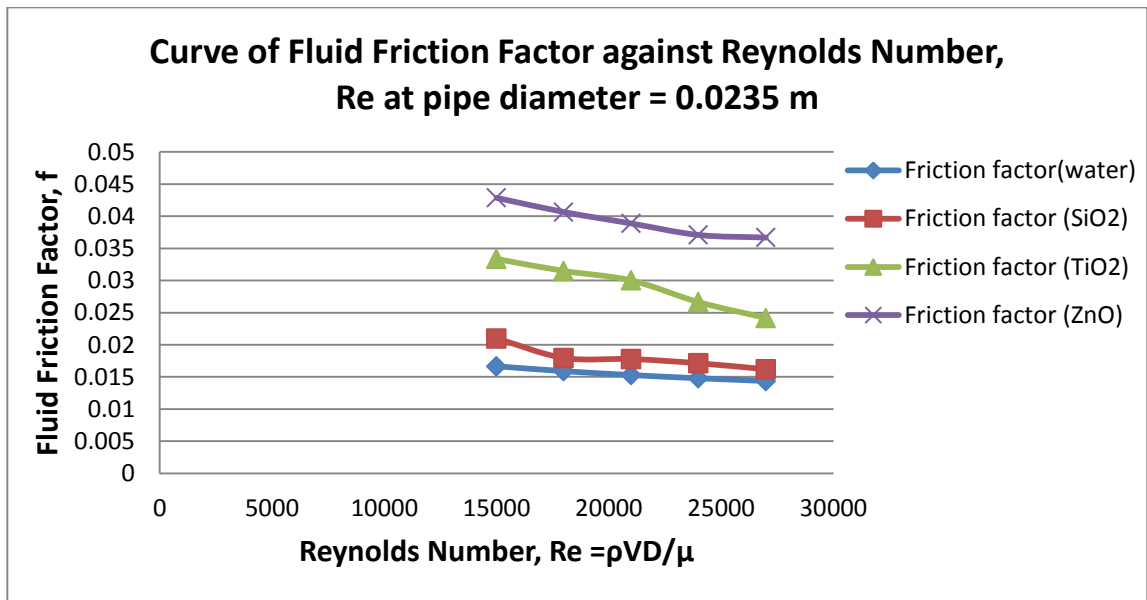


Figure 21. Curve of Fluid Friction Factor against Reynolds Number, Re at pipe diameter 0.0235 m

Table 8. Table of baseline data for fluid flow experiment for pipe diameter 13.3 mm

Medium diameter pipe (13.3 mm inner diameter)						
Flowrate (m ³ /h)	Pressure drop (mH ₂ O)	Characteristic length of pipe (m)	Hydraulic diameter (m)	Average velocity (m/s)	Gravitational acceleration (m/s ²)	Fluid friction factor, f
For SiO₂ nanofluids of 0.05 vol% concentration						
1.0	0.143	1	0.0235	1.9994	9.81	0.00932
1.2	0.198	1	0.0235	2.3993	9.81	0.00898
1.4	0.247	1	0.0235	2.7992	9.81	0.00824
1.6	0.325	1	0.0235	3.1991	9.81	0.00829
1.8	0.403	1	0.0235	3.5990	9.81	0.00813
For TiO₂ nanofluids of 0.05 vol% concentration						
1.0	0.225	1	0.0235	1.9994	9.81	0.01471
1.2	0.314	1	0.0235	2.3993	9.81	0.01425
1.4	0.407	1	0.0235	2.7992	9.81	0.01356
1.6	0.524	1	0.0235	3.1991	9.81	0.01336
1.8	0.646	1	0.0235	3.5990	9.81	0.01301
For ZnO nanofluids of 0.05 vol% concentration						
1.0	0.316	1	0.0235	1.9994	9.81	0.02060
1.2	0.431	1	0.0235	2.3993	9.81	0.01953
1.4	0.558	1	0.0235	2.7992	9.81	0.01859
1.6	0.704	1	0.0235	3.1991	9.81	0.01796
1.8	0.907	1	0.0235	3.5990	9.81	0.01828

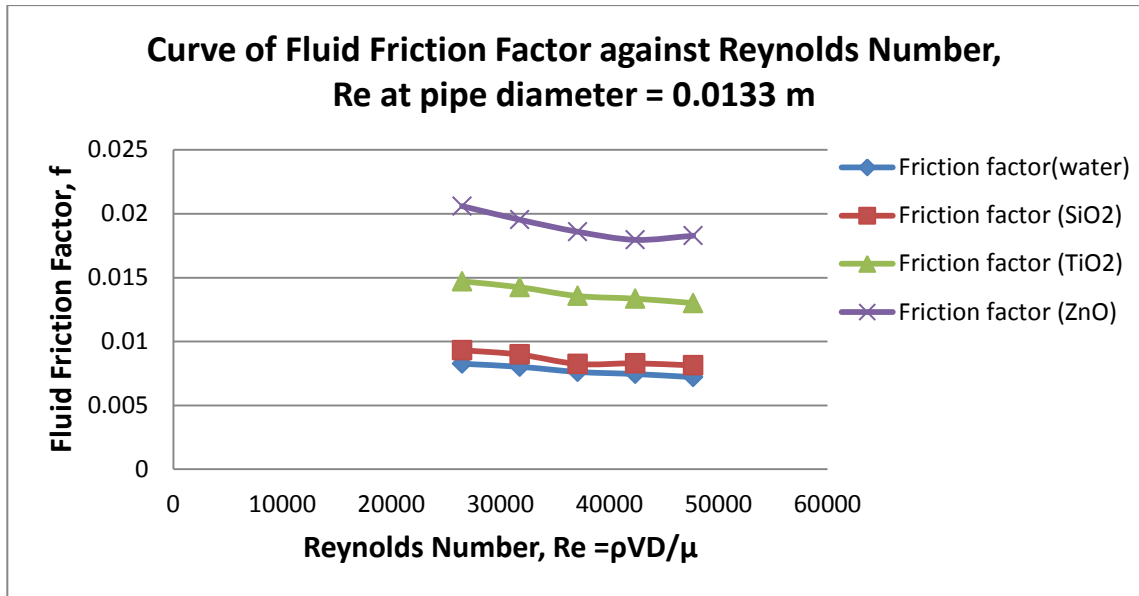


Figure 22. Curve of Fluid Friction Factor against Reynolds Number, Re at pipe diameter 0.0133 m

Table 9. Table of baseline data for fluid flow experiment for pipe diameter 8.5 mm

Medium diameter pipe (8.5 mm inner diameter)						
Flowrate (m ³ /h)	Pressure drop (mH ₂ O)	Characteristic length of pipe (m)	Hydraulic diameter (m)	Average velocity (m/s)	Gravitational acceleration (m/s ²)	Fluid friction factor, f
For SiO₂ nanofluids of 0.05 vol% concentration						
0.4	0.248	1	1.9581	1.9994	9.81	0.01077
0.6	0.504	1	2.9371	2.3993	9.81	0.00975
0.8	0.838	1	3.9162	2.7992	9.81	0.00911
For TiO₂ nanofluids of 0.05 vol% concentration						
0.4	0.411	1	1.9581	1.9994	9.81	0.01788
0.6	0.837	1	2.9371	2.3993	9.81	0.01619
0.8	-	1	3.9162	2.7992	9.81	-
For ZnO nanofluids of 0.05 vol% concentration						
0.4	0.492	1	1.9581	1.9994	9.81	0.02140
0.6	1.003	1	2.9371	2.3993	9.81	0.01938
0.8	-	1	3.9162	2.7992	9.81	-

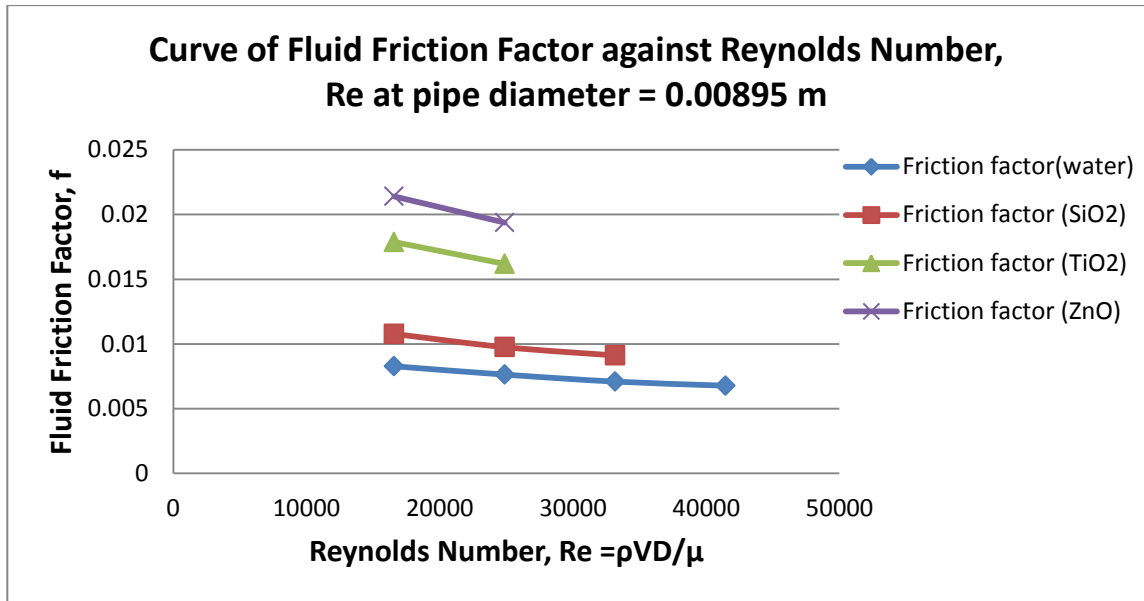


Figure 23. Curve of Fluid Friction Factor against Reynolds Number, Re at pipe diameter 0.00895 m

5.3 Discussion

The results as seen in figures 21, 22, and 23 has shown that in turbulent flow, the friction factor of nanofluids mirrors or approaches the pattern for baseline data (water) which shows a decreasing trend. This shows that inertial effects dominate shear stress as compared at turbulence rather than viscosity dominated shear stress prevalent along laminar flow. Since this study does not encompass laminar flow, effect of viscosity towards fluid friction factor cannot be determined. Further study needs to be done to investigate further viscosity effects towards friction factor as researched by Ko et al. (2007).

Most importantly, across all pipe diameters, ZnO nanoparticle which possess highest density shows highest value of fluid friction followed by TiO₂ and SiO₂. This pattern has proved that density does indeed affect fluid friction factor in a way that as nanoparticle density increases, fluid friction will also increase. Thus, one of the characterization requirements of nanofluid is density.

Friction factors for water shown in figure 20 although do not accurately in sync with the values indicated in Moody Chart and Colebrook equation formulation. However, values shown displays similar decreasing trend therefore indicating validation of experimental setup used.

It can be observed in figure 20 that the experimental baseline data is lower than the theoretical calculations by a significant margin albeit the theoretical values are devised with reference to smooth curve (relative roughness = 0) along Moody chart. This may be due to difference between calculated Reynolds number using average velocity evaluated from flow continuity equation, $Q = AV$ is different from the actual Re of the pipe flow. Since the experimental setup is very old and used quite rarely, scale buildup along the inside wall of the pipe may have reduced the effective diameter of the duct. Consequently, for a constant flowrate, as the effective duct area decreases, the velocity would increase and thus Reynolds would also increase. Therefore, it is recommended that in the future, prior to running the experiment the apparatus should be cleaned and serviced thoroughly.

It is also observed from figure 17 and 21 for theoretical modeling of experiment and actual experimental result respectively that the results differ quite substantially. This may be explained especially for the case of Zinc Oxide and Titanium Oxide that the nanoparticles have agglomerated hence causing coefficient of drag to vary along the flow line therefore producing inconsistent results for pressure drop. This can be prevented in the future by sonication as done by Ko et al. (2007) to deagglomerate and agitate particles so that the nanoparticles will be dispersed evenly.

Another factor that might affect data inconsistency is differing particle sizes for each nanoparticle. Nanoparticles procured from manufacturer come in a range of particle sizes for instance SiO₂ nanoparticles comes at a range between 5-30 nm. This variance in size might affect individual particle coefficient of drag which in turn produces a different or higher resultant friction factor than that of the theoretical model. One suggestion to tackle this issue is by first conducting X-Ray Diffraction (XRD) and Transmission Electron Microscopy (TEM) or Scanning Electron Microscope (SEM) to predetermine nanofluid constituents and average particle size so that theoretical calculations could be modelled fairly accurately.

Other than that, inconsistency might be resulting from incorrect manometer reading caused by undetected bubbles in manometer connection. Among preventive measures should be taken is to let the connection to be primed with fluid before taking a reading. In addition, other methods of measuring pressure drop such as differential pressure transducers for a more precise measurement.

CHAPTER 6

CONCLUSION AND RECOMMENDATIONS

Based on the results of this study, it can be confirmed that density is one of the parameters affecting fluid friction factor in pipes for nanofluids. For a constant nanofluid concentration, as nanoparticle density increases fluid friction factor will also increase as shown by ZnO nanofluids which is the most dense nanoparticle yielding highest fluid friction factors followed by TiO₂ and SiO₂ at the same Reynolds number. Preparation methodology of nanofluids includes one-step method and two-step method, and prior to conducting the experiment, aqueous nanoparticle dispersions are diluted with water before being mixed using a mechanical mixer. Friction factors of ZnO, SiO₂, and TiO₂ are calculated using Darcy-Weisbach equation for pressure loss with values of pressure loss obtained from experiments conducted on fluid friction apparatus. Hence, objectives of the study are achieved.

Among suggested continuation of this study is to consider the effects of different particle sizes on fluid friction factor, analysis of nanofluids frictional drag in laminar flow to study effects of viscosity towards fluid friction and also to conduct X-Ray Diffraction (XRD) and Transmission Electron Microscopy (TEM) or Scanning Electron Microscope (SEM) on the nanofluids to find out the average particle size for a given range of nanoparticle size.

References

- BBC. (2014). *Silicon dioxide*. Retrieved November 25, 2014, from [bbc.co.uk: http://www.bbc.co.uk/schools/gcsebitesize/science/add_ocr_pre_2011/chemicals/rocksm_ineralsrev3.shtml](http://www.bbc.co.uk/schools/gcsebitesize/science/add_ocr_pre_2011/chemicals/rocksm_ineralsrev3.shtml)
- Benhebal, H., Chaib, M., Salomon, T., Geens, J., Leonard, A., Lambert, S. D., et al. (2013). Photocatalytic degradation of phenol and benzoic acid using zinc oxide powders prepared by sol gel process. *Alex. Eng. J.*, 517-523.
- Chang, H. T., Tsung, T. T., Chen, L. C., Yang, Y. C., Lin, H. M., Lin, C. K., et al. (2005). Nanoparticle suspension preparation Using the Arc Spray Nanoparticle Synthesis System Combined with Ultrasonic Vibration and Rotating Electrode. *The International Journal of Advanced Manufacturing Technology* 26, 552-558.
- Choi, S. (1998). Nanofluid technology: current status and future research. *Korea U.S. Technical Conference on Strategic Technologies*. Vienna, VA.
- Choi, S. U. (1995). Enhancing thermal conductivity of fluids with nanoparticles, in *Developments and Applications of Non-Newtonian Flows. ASME FED 231/MD (66)*, 99-103.
- Choi, S., Zhang, Z. G., Yu, W., Lockwood, F. E., & Grulke, E. A. (2001). Anomalously Thermal Conductivity Enhancement in Nanotube Suspensions. *Applied Physics Letters* 79, 2252-2254.
- Das, A., Wang, D. Y., Leuteritz, A., Subramaniam, K., Greenwell, H. C., Wagenknecht, U., et al. (2011). Preparation of zinc oxide free, transparent rubber nanocomposites using a layered double hydroxide filler. *J. Mater. Chem.*, 7194-7200.
- Das, S. K., Choi, S. U., Yu, W., & Pradeep, T. (1998). *Nanofluids: Science and Technology*. Hoboken, NJ: John Wiley & Sons.
- Flörke, O. W. (2008). Silica. *Ullmann's Encyclopedia of Industrial Chemistry*. Weinheim: Wiley-VCH.
- Greenwood, N. N., & Earnshaw, A. (1984). In *Chemistry of the Elements* (pp. 1117-19). Oxford: Pergamon Press.
- Greenwood, N. N., & Earnshaw, A. (1997). *Chemistry of the Element (2nd ed.)*. Butterworth-Heinemann.
- Hawk's Perch Technical Writing. (n.d.). *Silica Nanoparticles*. Retrieved November 25, 2014, from UnderstandingNano.com: <http://www.understandingnano.com/silica-nanoparticles.html>
- Iler, R. (1979). *The Chemistry of Silica*. Plenum Press.

- Klingshirn, C. (2007). ZnO: Material, Physics and Application. *ChemPhysChem* 8 (6), 782-803.
- Ko, G. H., Heo, K., Lee, K., Kim, D. S., Kim, C., Sohn, Y., et al. (2007). An experimental study on the pressure drop of nanofluids containing carbon nanotubes in a horizontal tube. *International Journal of Heat and Mass Transfer* 50, 4749–4753.
- Kołodziejczak-Radzimska, A., & Jesionowski, T. (2014). Zinc Oxide—From Synthesis to Application: A Review. *Materials — Open Access Materials Science Journal*.
- Kostic, M. (n.d.). *Nanofluids: Advanced Flow and Heat Transfer Fluids*. Northern Illinois University, IL.
- Little, J. (n.d.). *Uses/Acquirement of Silicon Dioxide*. Retrieved November 25, 2014, from Silicon DioXide:
http://web1.caryacademy.org/facultywebs/gray_rushin/StudentProjects/CompoundWebSites/2003/silicondioxide/Uses.htm
- Ma, H. B., Wilson, C., Bogmeyer, B., Park, K., Yu, Q., Choi, S., et al. (2006). Effect of nanofluid on the heat transport capability in an oscillating heat pipe. *Applied Physics Letters, lett.88 143116*, 1-3.
- Munson, B. R., Young, D. F., Okishii, t. H., & Huebesh, W. W. (2010). *Fundamentals of Fluid Mechanics*. Hoboken, NJ: John Wiley & Sons.
- Nikuradse, J. (1933). Stroemungsgesetze in rauhen Rohren. *Ver. Dtsch. Ing. Forsch.*, 361.
- Nishi, Y., & Doering, R. (2007). *Handbook of Semiconductor: Manufacturing Technology*. CRC Press.
- Porter, F. (1991). *Zinc Handbook: Properties, Processing, and Use in Design*. CRC Press.
- Riordan, M. (n.d.). The Silicon Dioxide Solution: How physicist Jean Hoerni built the bridge from the transistor to the integrated circuit. *IEEE Spectrum*.
- Romano, J. M., Parker, J. C., & Ford, Q. B. (1997). Application Opportunities for Nanoparticles Made from Condensation of Physical Vapor. *Advances in Powder Metallurgy and Particulate Materials* 2, 12-3.
- Routbort, J. (2009). *Nanofluids Industrial Cooling*. Retrieved August 12, 2014, from U.S. Department of Energy:
http://www1.eere.energy.gov/industry/nanomanufacturing/pdfs/nanofluids_industrial_cooling.pdf
- Schweiser Kosmetik-und Waschmittelverband (SKW). (2009). Sicherheit von Nanopartikeln in Sonnenschutzmitteln. *Stellungnahme*.
- Singh, D., Routbort, J., Chen, G., Hull, J., Smith, R., Ajayi, O., et al. (2006). *Heavy Vehicle Systems Optimization Merit Review and Peer Evaluation*. Argonne National Lab.

- Steinbach, C. (n.d.). *Titanium Dioxide-Material Information*. Retrieved November 25, 2014, from DaNa2.0: <http://www.nanopartikel.info/en/nanoinfo/materials/titanium-dioxide>
- Sundar, L. S., Farooky, M. H., Sarada, S. N., & Singh, M. K. (2013). Experimental thermal conductivity of ethylene glycol and water mixture based low volume concentration of Al₂O₃ and CuO nanofluids. *International Communications in Heat and Mass Transfer* 41, 41-46.
- Weir, A., Westerhoff, P., Fabricius, L., & Von Goetz, N. (2012). Titanium Dioxide Nanoparticles in Food and Personal Care Products. *Environmental Science & Technology*, 46(4), pp. 2242-2250.
- Wiberg, E., & Holleman, A. F. (2001). *Inorganic Chemistry*. Elsevier.
- Wong, K. V., & De Leon, O. (n.d.). *Applications of Nanofluids; Current and Future*. Coral Gables, FL: University of Miami.
- Yu, W., France, D. M., Choi, S. U., & Routbort, J. L. (2007). *Review and Assessment of Nanofluid Technology for Transportation and Other Applications*. Argonne, IL: US Department of Energy.
- Yuan, Z., Zhou, W., Hu, T., Chen, Y., Li, F., Xu, Z., et al. (2011). Fabrication and properties of silicone rubber/ZnO nanocomposites via in situ surface hydrosilylation. *Surf. Rev. Lett.*, 33-38.

Appendix

Properties of nanoparticles in the order of decreasing density

Nanoparticle	Thermal Conductivity, W/m K	Density, kg/m ³	Specific heat, J/kg K
Cu	383	8954	386
CuO	69	6350	535
ZnO	29	5600	514
ZrO ₂	1.7	5500	502
Fe ₃ O ₄	6	5180	670
TiO ₂	8.4	4175	692
Al ₂ O ₃	36	3920	773
SiC	490	3160	675
SiO ₂	1.4	2220	745